Korean J. Chem. Eng., 34(5), 1328-1336 (2017)
DOI: 10.1007/s11814-017-0035-z

pISSN: 0256-1115
eISSN: 1975-7220

Laminar flow and chaotic advection mixing performance in a static mixer with perforated helical segments

Huibo Meng, Xiuhui Jiang, Yanfang Yu†, Zongyong Wang, and Jianhua Wu

Engineering and Technology Research Center of Liaoning Province for Chemical Static-Mixing Reaction, School of Energy and Power Engineering, Shenyang University of Chemical Technology, Shenyang 110142, P. R. China
(*Received 27 December 2016 • accepted 6 February 2017*)

Abstract−The laminar flow and chaotic mixing characteristics of a high-viscosity fluid in static mixers with staggered perforated helical segments were numerically investigated in the range of Re=0.1-150. The numerical results of pressure drop of Kenics static mixer have a good agreement with the reported data from the literature. The effects of aspect ratio A_r and Reynolds number on the mixing performance of Modified Kenics Static Mixers (MKSM) were evaluated by Darcy friction coefficient, shear rate, stretching rate, and Lyapunov exponent, respectively. The product of f×Re for MKSM linearly increased with the increase of Re, but it was constant under Re<10. The values of shear rate in the first perforated hole of mixing elements gradually became much larger by 1.10%-11.78% than those in the second perforated hole with the increasing Re. With the increase of dimensionless axial mixing length, the stretching rate increased linearly and the sensitivity for initial condition gradually weakened. A larger A_r is beneficial for micro-mixing in creeping flow. The average Lyapunov exponent linearly increases with the increase of Re. The profiles of Lyapunov exponent at different dimensionless perforated diameter (d/W) and perforated spacing (s/W) indicate that the chaotic mixing in MKSM is much more sensitive to d/W than s/W. A dimensionless parameter η taking into account the mixing degree and pressure drop was employed to evaluate the mixing efficiency. The optimization of perforated helical segments with the highest mixing efficiency at Re=100 was d/W=0.55 and s/W=1.2.

Keywords: Perforated Helical Segments, Chaotic Advection, Darcy Friction Coefficient, Shear Rate, Lyapunov Exponent

INTRODUCTION

Mixing of fluids plays a critical role in the success or failure of many industrial processes where a defined degree of homogeneity of a mixture is required [1,2]. Ordinary mixing devices are dynamic mixers for agitated stirrers in batch operations and static mixers for inline mixing in continuous operations [3].

Static mixers can accomplish many mixing tasks by the pressure drop between inlet and outlet solely [4]. Therefore, static mixers are widely used in many processing applications, such as polymer blending, food processing, minerals processing, water and wastewater treatment, homogenization, chemical reaction, heat and mass transfer process, and so on. These applications can be divided into four types: blending of miscible fluids, generating immiscible fluid interface, heat transfer, and blending solids [4,5]. Some of the advantages of static mixers over dynamic mixers are that they have no moving parts, low maintenance and operating cost, low space requirements, a short residence time, and easy installation. Static mixers are available for different working conditions, i.e., laminar, transitional and turbulent flow regimes.

The typical Kenics static mixer (KSM) is composed of a number of mixing elements which have alternating clockwise or counterclockwise directions of twist, and the leading edge of each element is offset by 90° relative to the trailing edge of the preceding one [6]. The mixing elements are designed to create secondary flows to mix different fluid streams as they flow through the static mixer [3]. Hobbs and Muzzio [7-10] used Lagrangian methods to characterize the laminar flow and mixing performance of KSM. The effects of Reynolds number, twist angle of elements and injection location were evaluated, respectively. The injection location strongly affected the extent of mixing only for the first few elements in the standard KSM. The flow in the static mixer with the same twist direction elements displayed two oval-shape regions, which acted as a barrier to uniform mixing. A substantial increase in mixing efficiency is achieved using elements with less twist than the standard 180° Kenics configuration. The globally chaotic flow and mixing performance was independent of Re for creeping flow conditions and the flow was predominantly chaotic again except for small islands remained at Re=1000. Fourcade et al. [11] developed a new method to calculate the average rate of striation thinning in the laminar flow field of a KSM. Rahmani et al. [12] numerically simulated the mixing processes of single-phase viscous liquids in KSM at different Re. Their work showed that the effect of Re on mixing in creeping flow was minimal, but the Re had a major impact on the mixing performance of a static mixer in laminar and turbulent flows. Furthermore, they also found that the predictions of k-ω turbulent model needed more computational time and could get more than enough accuracy than those of RSM turbulent model. Rahmani et al. [1] numerically analyzed the mixing properties of pseudoplastic fluids in KSM and found that the carboxymethyl

†To whom correspondence should be addressed.
E-mail: taroyy@163.com

cellulose fluid was not effective on the degree of mixing. Lisboa et al. [13] found that the numerical results of supercritical flow and heat transfer using RNG k-ε model were closer to the experimental data than the predictions from standard k-ε and k-ω models under high pressure condition. Saatdjian et al. [14] numerically studied chaotic advection and mixing in a spatially periodic flow. The initial location of a blob of dye was important for its spreading over the cross section only in the first few mixing elements and its influence decreased afterwards. Kumar et al. [15] numerically and experimentally studied the flow patterns and mixing performance of KSM over a wide range of Re=1-25 000. The pressure drop per unit element was found to be independent of the number of mixing inserts and the effect of element-to-element transition on flow took up to 30% of the element length. To simulate the evolution of the drop size distribution (DSD) in liquid-liquid systems, the population balance equation (PBE) was coupled with the multi-phase description and added to the standard equations in the CFD code with proper kinetic expressions for the breakage rate. Instead of solving the original PBE, transport equations for the moments of the DSD were solved and the closure problem was overcome by using the quadrature method of moments (QMOM) [16].

Tajima et al. [17] proposed a new method to release liquid CO_2 into the ocean at intermediate depths in a submerged KSM. The mixing functions of static mixer on CO_2 hydrate formation were experimentally carried out, and the variations in size and distributions of CO_2 drops were investigated using a statistical method [18,19]. The temperature-sensitive monomer N, N-diethylacrylamide and photo-crosslinkable pre-polymer ENT were used as model hydrogel materials [20]. The laminar flow conditions in KSM were compared with the behavior of flows in coiled tubes and in tubes with twisted tape inserts. For easier comparison, a modified Dean number was proposed and the existence of secondary flow in tubes with helical static elements was proved by Ujhidy et al. [21].

In the past decades, some other static mixers have been developed and applied into the chemical industry process [22-26]. Regner et al. [3] numerically investigated the mixing processes in Lightnin Series 45 static mixer (LSM) using Z factor, helicity and the rate of striation thinning. Regner et al. [2] employed the VOF method to analyze the two liquids mixing processes and found that the mixing performance was lower with greater difference in viscosity. The flow performance and mixing characteristics of a high-viscosity fluid in static mixers with radial multitwisted and axial twisted tapes were numerically investigated based on Lagrangian tracking method [27,28]. The chaotic mixing performance was evaluated by the particle distribution maps, extensional efficiency and stretching rate. Yu et al. [29] numerically investigated the laminar characteristics of heat transfer and friction factor in a circular tube equipped with two Q-type inserts.

It is challenging to design good static mixers taking into consideration the two aspects of low pressure drop and efficient mixing. The thermal performance of static mixer with staggered perforated twisted tapes was superior to that of the tube with typical twisted tapes in turbulent flow [30,31]. Many fluids used in the industrial processes are high-viscosity fluids, and the mixing performance of high viscosity fluids plays an important role in food process, chemical engineering process, and the pharmaceutical industry [32]. Therefore, it is interesting and meaningful to investigate the mixing process of high-viscosity fluids in the industry process [4,5,33].

The laminar flow and chaotic mixing performance of a high-viscosity fluid in static mixers with perforated helical segments were numerically investigated by the academic CFD software package-ANSYS Fluent R16.1 in the range of Re=0.1-150. The effects of aspect ratio A_r and Re on mixing performance were evaluated by friction coefficient, mean shear rate, stretching rate, and Lyapunov exponent, respectively.

NUMERICAL METHODOLOGY

1. Governing Equations

The general assumptions under the current condition are considered to be three-dimensional with constant fluid properties. In the case of incompressible flow, the mass continuity equation is simplified to a volume continuity equation:

$$\nabla \cdot \mathrm{u} = 0 \tag{1}$$

where u is the velocity vector.

The momentum conservation equation in the static mixers with perforated helical segments can be written as follows:

$$\frac{\partial(\rho \mathrm{u})}{\partial \mathrm{t}} + \nabla \cdot (\rho \mathrm{uu}) = -\nabla \mathrm{p} + \nabla \cdot (\tau) + \mathrm{F} \tag{2}$$

where ρ is the fluid density, t is the time, p is the static pressure, τ is the stress tensor, and F is external body forces.

The governing equations in Cartesian coordinates were discretized on an unstructured grid using a finite-volume approach. A pressure-based solver was employed with a second implicit scheme for incompressible flows in the static mixers. The well-known SIMPLEC algorithm was used to deal with the pressure-velocity coupling between the momentum and the continuity equations of steady incompressible flows in the static mixers with perforated helical segments. The green-gauss cell based, standard, and second-order upwind schemes were employed for gradient, pressure, and momentum discretization, respectively. The normalized residuals for the continuity and momentum equations were lower than 1×10^{-5} and 1×10^{-6}, respectively. The numerical cases were performed in a Dell PowerEdge R815 server.

2. Geometry Model and Fluid Properties

We constructed a series of the novel modified Kenics static mixers (MKSM) to improve the understanding of how static mixers work in laminar flow. As shown in Fig. 1, the modified Kenics blades has an aspect ratio of A_r=1.5 which is equal to the length l to width w. The MKSM is usually composed of a number of staggered perforate Kenics blades with a twist angle of 180° and a rotation of 90° relative to the previous one [31]. The rectangular plates are drilled with two symmetrical perforated holes with a spacing of s and a diameter of d, and then twisted with an angle of 180°. So, the holes in the twisted blades become lachrymiform. The geometric parameters of MKSM and fluid properties are given in Table 1.

3. Boundary Conditions

The governing equations in the laminar flow were discretized

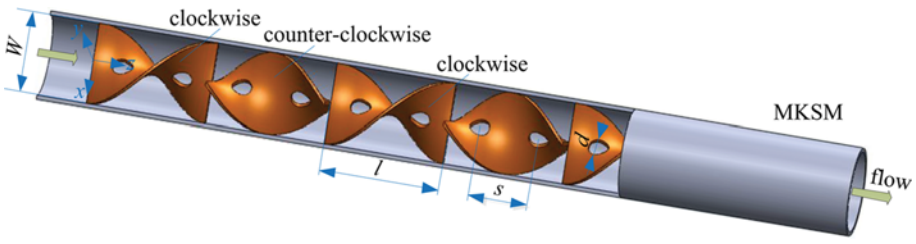

Fig. 1. Static mixers with staggered modified Kenics blades.

Table 1. Geometrical parameters of MKSM and fluid properties

Geometrical parameter	MKSM		
Tube diameter, D (m)	0.04		
Blade length, l (m)	0.04	0.06	0.08
Blade width, W (m)	0.04		
Blade thickness, δ_b (m)	0.002		
Perforated diameter, d (m)	0.010-0.030		
Perforated hydraulic diameter, d_h (m)	0.095-0.0294		
Perforated spacing, s (m)	0.012-0.068		
Aspect ratio, A_r	1	1.5	2
Twist angle, θ (deg)	180		
Entrance length l_i (m)	0.025		
Mixing-zone length l_m (m)	0.48	0.72	0.96
Exit length, l_o (m)	0.025		
Fluid properties			
Density, ρ (kg/m^3)	1200		
Viscosity, μ (kg/m·s)	0.5		

and solved by the finite volume method using the academic ANSYS Fluent R16.1. The user-defined functions (UDF) were compiled and loaded to generate the parabolic profiles for fully developed laminar flow in the smooth inlet sections. The Reynolds number for entrance is defined as

$$\mathrm{Re}=\frac{\rho \mathrm{Du}}{\mu} \tag{3}$$

where D is the diameter of the tube, and μ is the viscosity of the fluid. The inlet velocity employed in the simulations is in the range of $u=1.04\times10^{-4}$-1.56×10^{-1} m/s. In other words, Re ranges from 0.1 to 150. The reference pressure point is located at the geometric center of the outlet section where boundary condition is set as outflow. No-slip boundary conditions are applied on the tube wall and on the surface of the blades of the static mixers.

4. Model Validation and Grid Independence Test

In the velocity-pressure formulation for CFD analysis, pressure is more sensitive to spurious oscillations than velocity and concentration [34]. Therefore, the computational precision of three-dimensional velocity field is dependent on the pressure field's accuracy [27]. The CFD model of static mixer fitted with staggered Kenics blades was validated by comparing the predicted results of pressure drop Δp against the available literature data [15,34,35]. It is clearly seen in Fig. 2(a) that the numerical results have a good agreement with the empirical correlations.

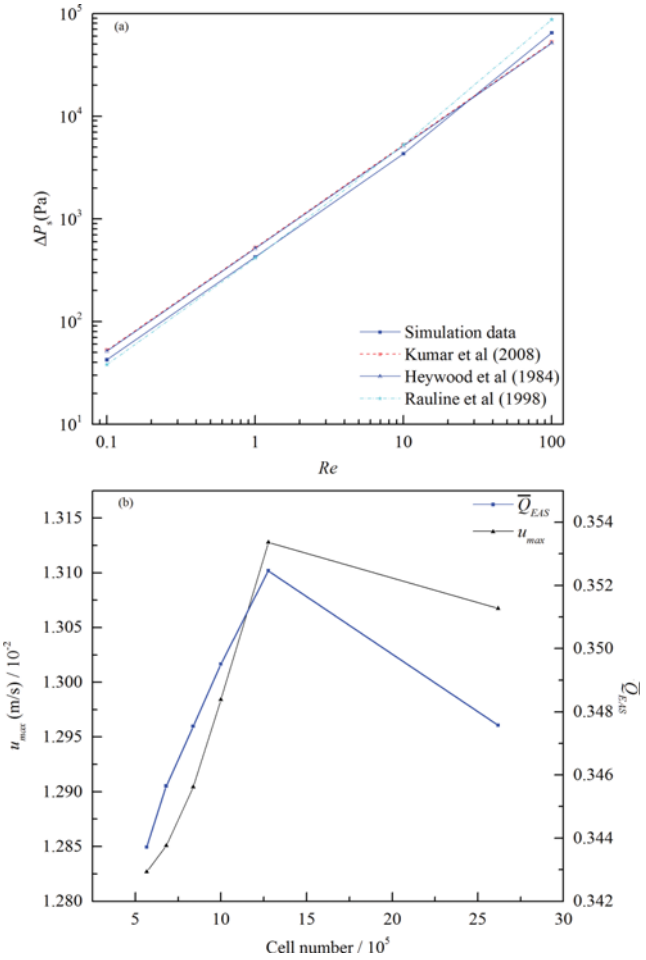

Fig. 2. Mesh validation and grid independence test. (a) Comparison of pressure drops of KSM between the numerical result and literature data, and (b) The profiles of average QEAS value and the maximum of x-velocity for different cell numbers.

The three-dimensional models of different static mixers constructed by SolidWorks were imported into Gambit for grid meshing. Unstructured tetrahedral meshes were used to discretize the computational domain. To determine the grid independence, 2618194, 1276806, 999127, 837446, 680774 and 567274 cells were generated, respectively, for the MKSM with A_r=1.5. The grid quality was checked for EquiAngle skew. As illustrated in Fig. 2(b), the average Q_{EAS} value of MKSM with 1276806 cells is the largest and nearest to 0.4, which indicates the case has higher quality meshes [36]. As shown in Fig. 2(b), the maximum of *x*-directional veloc-

ity in the line from (0, −20 mm, 330 mm) to (0, 20 mm, 330 mm) firstly increases quickly and then decreases with the increase of cell number. It is obviously seen that the maximum of *x*-directional velocity in the model with 1276806 cells is the largest. On the other hand, the computation time of the numerical case with 2618194 cells is 3-4 times longer than that of the case with 1276806 cells. Taking into account the grid independence and computation accuracy, the three-dimensional model with a number of 1276806 cells were carried out in the CFD simulation.

RESULTS AND DISCUSSION

1. Friction Factor

In fluid dynamics, the Darcy friction factor is also known as the Darcy-Weisbach friction factor, resistance coefficient or simply friction factor for the description of pressure drop in pipe flow as well as open-channel flow. Generally, the friction factor is four-times larger than the Fanning friction factor and could be defined as follows [37]

$$f=\frac{2D\Delta p}{\rho \overline{u}^2 l_m} \tag{4}$$

where Δp is the pressure drop across the mixing elements.

It is well known that the swirling flow becomes more significant in the MKSM because of the helicity of mixing segments. With a given Re, in Fig. 3(a) the friction factor in MKSM clearly firstly increases quickly from z/*l*=1 to z/*l*=2, then slowly increases from z/*l*=2 to z/*l*=6, and has a variation less than 1% for z/*l*>6. On the other hand, the friction factor decreases with the increasing A_r as shown in Fig. 3. From Fig. 3(a), the friction factor in MKSM with A_r=2.0, 1.5, 1.0 is 6.11, 8.49 and 16.95 times as large as that in a circular pipe at Re=100 and z/*l*=12, respectively. It is noted in Fig. 3(b) that the Darcy friction factor values firstly decrease sharply in the creeping flow and then gradually decrease because the l force begins to play a more important role with the increase of Re. Furthermore, the ratios of friction factor in MKSM with A_r=2.0, 1.5, 1.0 to that in the smooth tube are in the range of 4.64-7.11, 5.65-10.49, 8.29-22.82, respectively. Taking into account the mixing desire and pressure drop, it is necessary to employ an MKSM with A_r=1.5-2 for common mixing operations. According to the classical theory prediction for laminar flow in smooth circle tubes, the product between Darcy friction factor and Re is constant [29]. For Re≥10, the product of f×Re in MKSM linearly increases with the increase of Re as illustrated in Fig. 3(c). Nevertheless, the product of f×Re in the creeping flow of MKSM with different A_r under Re<10 has different constant values.

2. Shear Rate

The level of shear rate is an indication of the dispersive capability of a mixer to break up solids agglomerates, drops, and bubbles [38,39]. It is obviously flow rate-dependent and defined as follows [40]:

$$\gamma=\sqrt{\frac{1}{2}\overline{D}:\overline{D}} \tag{5}$$

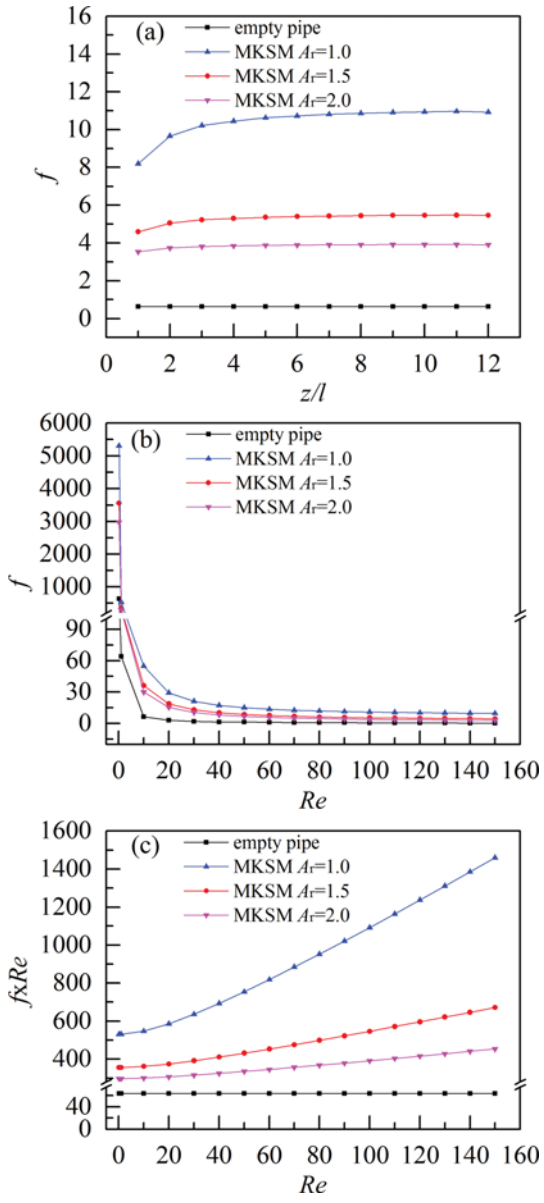

Fig. 3. The relationship between friction coefficient and Reynolds numbers.

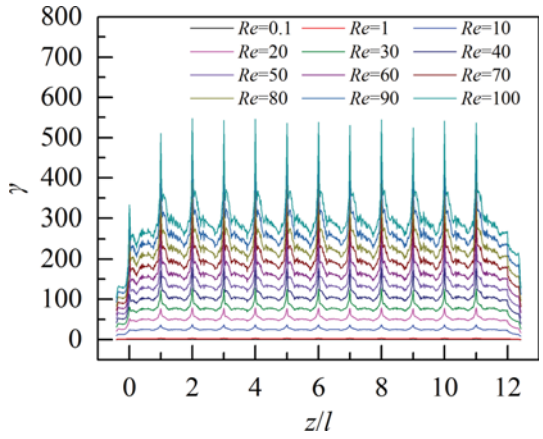

Fig. 4. The profiles of cross-sectional average shear rate of MKSM with A_r=1.5.

where $\overline{D}$ represents the rate of deformation tensor and is calculated by the following equation:

$$\overline{D}=\left(\frac{\partial u_j}{\partial x_i}+\frac{\partial u_i}{\partial x_j}\right) \quad (6)$$

Fig. 4 depicts the profiles of shear rate of MKSM with A_r=1.5 as a function of dimensionless axial position in the range of Re=0.1-100. For Re≤1, the norm values of rate of deformation tensor approach a constant value. For Re>1, the existence of perforated mixing segments begins to enhance the mixing performance. The contributions of the first leading and the last ending edges on shear rate are less than those of the segment transitions. On the other hand, the values of shear rate in the wake regions decrease sharply and approach the values of smooth tube.

The average values of shear rate in the mixing elements and transition regions are 2.60-2.98 and 3.55-5.26 times of that in the smooth inlet, which indicates that the dispersive capability is largely enhanced. It can be clearly seen that the higher values of shear rate could be attained at higher Re, which indicates that better dispersive mixing could be obtained with higher flow rates. Furthermore, the values of shear rate in the first perforated hole of mixing elements gradually become much larger by 1.10%-11.78% than those in the second perforated hole with the increasing Re. It indicates that the perforated structure before the segments transition produces an acceleration flow through the triangle regions for downstream flow which obviously enhances the secondary flow.

3. Micro-mixing Performance

Saatdjian et al. [14] used the particle tracking technology to present a numerical study of chaotic advection and mixing in a spatially periodic, three-dimensional flow. It is well known that the mixing of fluids involves stretching and folding of material elements. The stretching rate determines the rate of the micro-mixing process, both by increasing the inter-material area over which inter-diffusion of components can occur, and by decreasing the required diffusional distance.

According to Ottino's theory [41], the coordinate positions and stretching of massless particles could be monitored by integrating and solving the following equations:

$$\frac{dz}{dt}=u(z) \quad z_{t=0}=z_0 \quad (7)$$

$$\frac{dI}{dt}=(\nabla u)^T\cdot I \quad I_{t=0}=I_0 \quad (8)$$

where z, I, and ∇u denote the position vector, stretching vector related to the massless particle and velocity gradient, respectively. In this study, an vector of I_0=(0, 0, 1) was employed to initialize the stretching value. The total accumulated stretching λ experienced by the element after some time is calculated based on the following equation:

$$\lambda=\frac{|I|}{|I_0|} \quad (9)$$

At a given cross section, the stretching rate is derived from the logarithms of geometric mean of accumulated stretching values for all massless particles [34,42]:

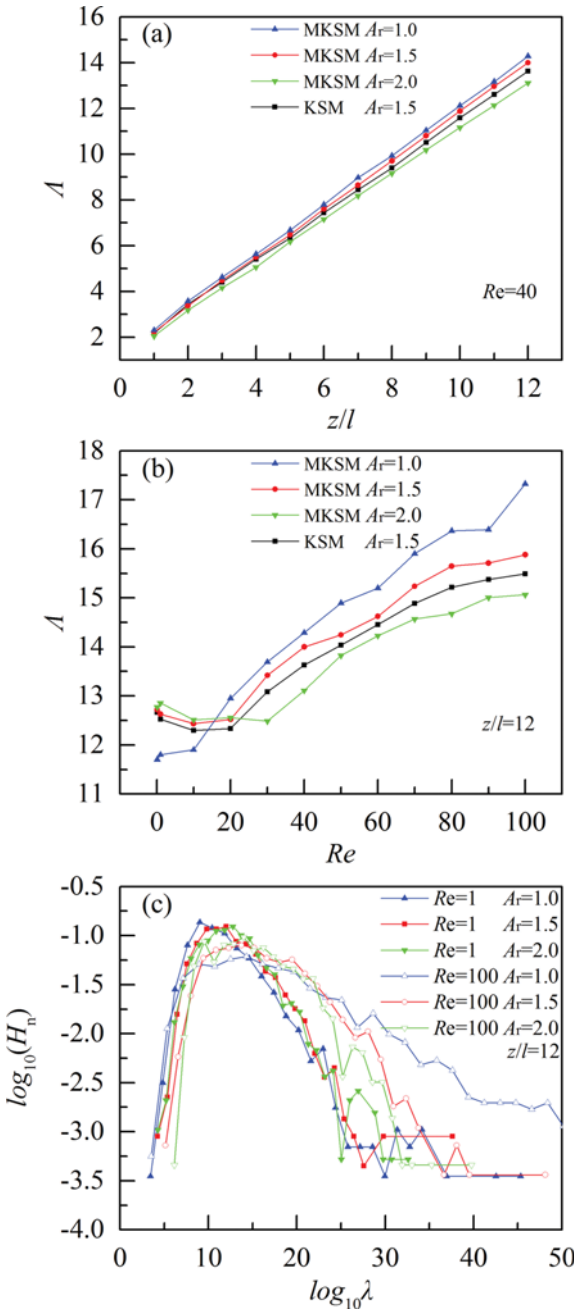

Fig. 5. The profiles of stretching rate of perforated static mixers. The effects of (a) z/*l* and (b) Re on stretching rate, and (c) Probability density distribution of stretching rate at z/*l*=12.

$$\Lambda=\log_{10}\left(\prod_{i=1}^{N}\lambda_i\right)^{1/N} \quad (10)$$

where N represents the number of massless particles passed through the given cross-section.

The profiles of stretching rate in the perforated static mixers under different Reynolds numbers are plotted in Fig. 5. The positions of massless particles experiencing high and low stretching correspond to regions of good and poor micro-mixing, respectively. As shown in Fig. 5(a), the stretching rate linearly increases with the increase of dimensionless axial length. There exists a bend at z/*l*=2 in the

profiles for MKSM with three different A_r because the initial vectors are realigned to correspond to the principal stretching directions of the flow before the second element. The initial vector orientations are no longer important after the realignment of vectors directions, and Λ grows linearly with the increase of dimensionless axial positions. The stretching rate of the MKSM with A_r=1.5 is much larger than that of the KSM with A_r=1.5 with the increasing number of mixing elements.

As illustrated in Fig. 5(b), the profiles of Λ for MKSM with A_r= 1.0, 1.5 and 2.0 have a little difference. The variations of Λ in MKSM with A_r=1.5 and 2.0 first decrease until Re=10 and then increase in the range of Re=20-100. The Λ in MKSM with A_r=1.0 increases with the increase of Re. The MKSM with A_r=2.0 has the highest stretching efficiency in the range of Re=0.1-10. It is well known that the stretching rate is independent of Re in the creeping flow [10,27,28]. Thus, a larger A_r could provide a longer flow passage with a given diameter which would play a more important role in the stretching and unfolding of materials in the creeping flow. Nevertheless, the MKSM with A_r=1.0 has the highest stretching efficiency and the advantages of MKSM with less A_r become more and more obvious in the range of Re=20-100. Therefore, the MKSM with A_r=1.0 can be chosen to achieve a mixing task in the range of Re=20-150. With the increasing Re, the micro-mixing performance of the MKSM with A_r=1.5 is larger than that of the KSM with A_r=1.5.

The statistical characteristics of stretching magnitudes provide a means for characterizing the distribution of mixing intensities within the flow field. The probability density function (PDF) of the logarithm of stretching rate is defined as follows [7,10,14]:

$$H_n(\log_{10}\lambda)=\frac{1}{N}\frac{dN(\log_{10}\lambda)}{d\log_{10}\lambda} \tag{11}$$

where $dN(\log_{10}\lambda)$ represents the number of particles having a stretching rate between $\log_{10}\lambda$ and $\log_{10}\lambda+d(\log_{10}\lambda)$, and the value of $H_n(\log_{10}\lambda)$ can be conducted as a spectral intensity measure of the micro-mixing process.

The statistical profiles of stretching rate at z/l=12 are plotted versus $\log_{10}\lambda$ at Fig. 5(c). The profiles of $H_n(\log_{10}\lambda)$ describing the spectrum of stretching in the bulk flow are similar and approach a bell shape with the increase of $\log_{10}\lambda$. As a result, the laminar mixing in MKSM is considered to be a chaotic flow as proposed by Liu et al. [43,44]. The $\log_{10}\lambda$ corresponding to the maxima of $H_n(\log_{10}\lambda)$ increases with the increase of A_r, which indicates that the MKSM with A_r=2.0 could achieve better micro-mixing for high-viscosity fluids in the creeping flow. When Re is much larger than 10, the statistical tendency of stretching rate in the MKSM becomes reverse. The coverage of $\log_{10}\lambda$ in the MKSM with A_r=1.0 under Re=100 becomes the largest and the maximum of $H_n(\log_{10}\lambda)$ becomes the minimum. Furthermore, more fluctuations are found in the areas with higher $\log_{10}\lambda$ values than those with lower $\log_{10}\lambda$ values. The curves also exhibit long tails on the high-stretching side, which indicates that a higher mixing degree could be attained in MKSM with smaller A_r.

4. Chaotic Mixing Characteristics

Stretching does not depend on velocity or tube diameter in the laminar regime. Material elements will be stretched in the same way at low or high velocity (or at large or small diameter), but the time needed to reach this stretching will be affected. The Lyapunov exponent is a signature of chaos, but it is also a characteristic of the mixing efficiency, the higher the exponent, the more chaotic the system, and the more efficient the mixer in principle [39]. The average Lyapunov exponent δ at cross sections can be calculated through the following relation:

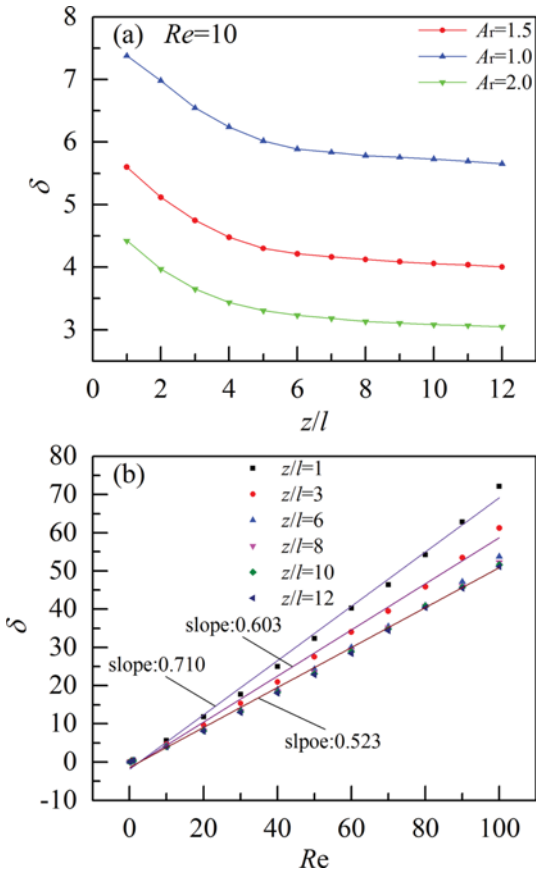

Fig. 6. Lyapunov exponent δ of static mixers as a function of (a) z/l for Re=10 and (b) Re for A_r=1.5.

$$\delta=\lim_{t\to\infty}\frac{\log_{10}\Sigma\lambda_i/N}{t} \tag{12}$$

The effects of aspect ratio and dimensional axial position on the Lyapunov exponent δ at Re=10 are plotted in Fig. 6(a). The average Lyapunov exponent for laminar flow is much larger than zero in an empty pipe. In Fig. 6(a) that the variation trends of Lyapunov exponent in the MKSM with A_r=1.0, 1.5, 2.0 are clearly similar. In other words, the Lyapunov exponent firstly decreases within the first six elements and then the decreasing rate becomes smaller from the sixth element to the ending element. That is, the homogeneous degree of mixing is gradually improved and the sensitivity for initial condition would be weakened with the increasing mixing elements. The aspect ratio of mixing elements plays an important role in the chaotic mixing performance. The Lyapunov exponent in MKSM with A_r=1.0 and 1.5 is 1.67-1.85 and 1.27-1.31 times of that in MKSM with A_r=2.0 at Re=10. Thus, the sensitivity for initial condition would be strengthened because sec-

ondary flow patterns become much stronger in the MKSM with less A_r.

Fig. 6(b) depicts the profiles of the average Lyapunov exponent δ at different cross sections of MKSM with A_r=1.5 with the increase of Re. The average Lyapunov exponent linearly increases with the increase of Re. The maxima of Lyapunov exponent could be obtained at the end cross section of the first element. With the increase of axial positions, the slope of increasing ratios gradually decreases from 0.710 to 0.523 and would not vary for z/l>6 as described in Fig. 6(b).

5. Optimization of Perforated Helical Segments

The existence of perforated holes generates an acceleration flow which may be beneficial to extension, shear and secondary flow. The effects of perforated diameter and spacing on chaotic mixing are evaluated by the average Lyapunov exponent in Fig. 7(a) and 7(b), respectively. From Fig. 7(a), in the MKSM with d/W=0.35 the minimum and maximum of Lyapunov exponent are attained at s/W=0.5 and s/W=1.5, respectively. Furthermore, two different regions can be clearly observed. It has been found that other curves are located far away from the curve with s/W=0.5. The worse mixing efficiency may be induced by the mismatching coupled effects between flow division and acceleration flow. As a result, it is considered as an unreasonable perforated structure with s/W=0.5 and d/W=0.35. As illustrated in Fig. 7(b), the effect of perforated diameter on chaotic mixing performance was evaluated. With the increase of perforated diameter, the mixing efficiency first decreases at d/W=0.3, then increases and decreases finally. The maximum values are attained at d/W=0.45 and the minima are obtained at d/W=0.75. The curves with d/W=0.75 are located away from other curves. That is because the helical flow passage is destroyed and the swirling flow is larger weakened when the perforated diameter is much larger.

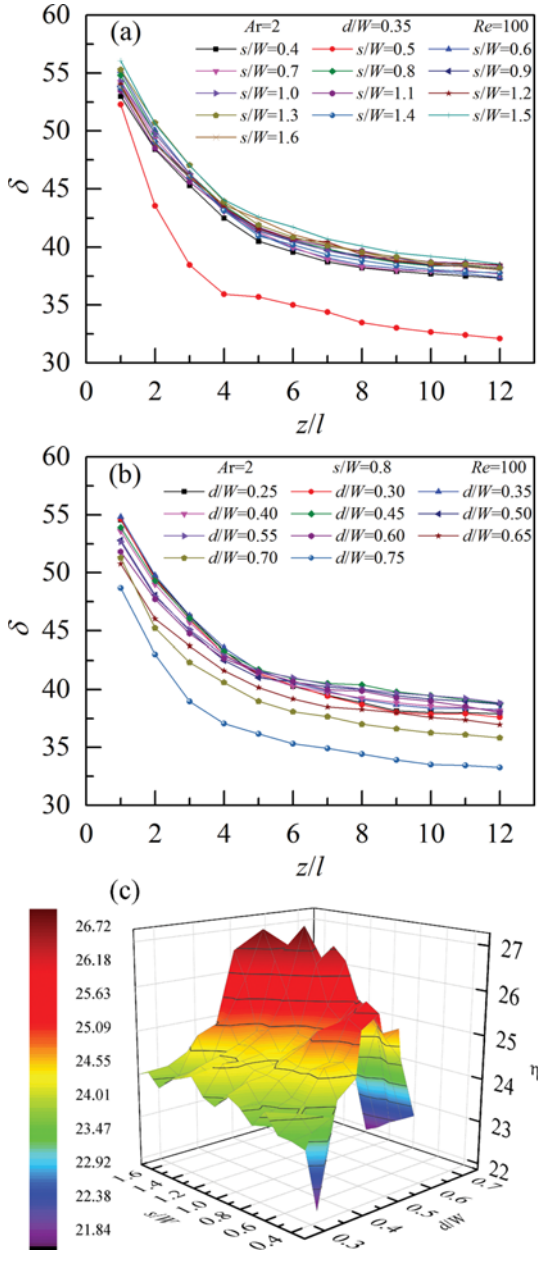

Fig. 7. The effects of (a) perforated spacing, and (b) perforated diameter on the distribution of Lyapunov exponent, and (c) the perforated optimization based on mixing performance factor.

The effects of perforated diameter and spacing on chaotic mixing are evaluated by the average Lyapunov exponent in Fig. 7(a) and 7(b), respectively. From Fig. 7(a), in the MKSM with d/W=0.35 the minimum and maximum of Lyapunov exponent are attained at s/W=0.5 and s/W=1.5, respectively. Furthermore, two different regions can be clearly observed. It has been found that other curves are located far away from the curve with s/W=0.5. The worse mixing efficiency may be induced by the mismatching coupled effects between flow division and acceleration flow. As a result, it is considered as an unreasonable perforated structure with s/W=0.5 and d/W=0.35. As illustrated in Fig. 7(b), the effect of perforated diameter on chaotic mixing performance was evaluated. With the increase of perforated diameter, the mixing efficiency first decreases at d/W=0.3, then increases and decreases finally. The maximum values are attained at d/W=0.45 and the minima are obtained at d/W=0.75. The curves with d/W=0.75 are located away from other curves. That is because the helical flow passage is destroyed and the swirling flow is larger weakened when the perforated diameter is much larger.

Comparison of the aforesaid profiles in Fig. 7(a) and 7(b), the chaotic mixing is much more sensitive to perforated diameter than perforated spacing. Thus, it is necessary to consider the coupled effect between perforated spacing and diameter on the mixing efficiency. Taking into account the tradeoff between increased mixing efficiency and friction factor, a dimensionless parameter η is similar with the one used in heat transfer field. The parameter η can be derived from the following equation:

$$\eta = \frac{\delta}{f^{1/3}} \tag{13}$$

From Fig. 7(c), the coupled effect on the mixing efficiency is obviously seen and the design of perforated mixing element is important for the mixing efficiency. The worst efficiency of chaotic mixing at Re=100 generates at d/W=0.35 and s/W=0.5, as shown in Fig. 7(a). The highest mixing efficiency at Re=100 could be attained at d/W=0.55 and s/W=1.2. Furthermore, some higher mixing efficiency could be obtained at d/W=0.5 and s/W=1.4 or d/W=0.6 and s/W=1.1.

CONCLUSIONS

The laminar flow and chaotic advection mixing performance of a high-viscosity fluid in the static mixer with perforated helical segments were numerically investigated by ANSYS Fluent R16.1. The numerical results of pressure drop for KSM with A_r=1.5 have a good agreement with the literature results. The effects of A_r and Re on the chaotic advection mixing performance were evaluated by several criteria: friction factor, shear rate, stretching rate, and Lyapunov exponent.

The products of f×Re for MKSM with A_r=1.0, 1.5, 2.0 linearly increased with the increase of Re for Re≥10, and nearly had different constant values under Re<10. The values of shear rate in the first perforated hole of the mixing elements gradually became much larger by 1.10%-11.78% than that in the second perforated hole with the increasing Re. It indicates that the perforated structure

before the segments produced an acceleration flow through the triangle regions for downstream flow which enhanced the secondary flow. The stretching rate increased linearly with the increase of dimensionless axial distance. A larger A_r is beneficial for micro-mixing in the creeping flow and a smaller A_r is beneficial for micro-mixing in the range of Re=20-100. The mixing efficiency of MKSM with A_r=1.5 was much larger than that of the KSM with A_r=1.5.

The Lyapunov exponent of MKSM decreased firstly within the first six elements and then the decreasing rates became smaller from the sixth element to the ending element. The homogeneous degree of mixing gradually was improved and the sensitivity for initial condition was weakened with the increasing mixing elements. The Lyapunov exponent of MKSM with A_r=1.0 had the smallest value, which indicates that MKSM with less aspect ratio of mixing segments had stronger secondary flow patterns.

The profiles of Lyapunov exponent at different s/W and d/W indicate that the chaotic mixing is much more sensitive to perforated diameter than perforated spacing. A dimensionless parameter η taking into account the micro-mixing efficiency and pressure drop was used to evaluate the mixing efficiency. The optimization of perforated helical segments with highest mixing efficiency at Re=100 was d/W=0.55 and s/W=1.2.

ACKNOWLEDGEMENT

This work was supported by the National Natural Science Foundation of China (grant numbers 21476142, 21306115 and 21106086), the Program for Liaoning Excellent Talents in University (grant number LR2015051), Liaoning Natural Science Foundation (grant number 201602594), the Higher Education Program Funds for the Key Laboratory Research of Liaoning Province (grant number LZ2016001), the Planning Program of Shenyang Science and Technology Bureau (No. F12-188-9-00), and Liaoning BaiQianWan Talents Program (grant number 2013921047).

NOMENCLATURE

A_r : aspect ratio of mixing element
d_h : the perforated hydraulic diameter [m]
D : the diameter of tube [m]
$\overline{D}$: the rate of deformation tensor
d : the perforated diameter [m]
f : friction coefficient
F : external body force [N]
$H_n(\log_{10}\lambda)$: probability density function of the logarithm of stretching rates
I : stretching vector
l : the length of mixing element [m]
l_i : entrance length [m]
l_m : the mixing-zone length [m]
l_o : exit length [m]
N : the average particle number of grid cell
p : static pressure [Pa]
Δp : pressure drop in static mixer [Pa]
Q_{EAS} : the quality of EquiAngle skew
Re : Reynolds number
s : the perforated spacing [m]
t : time [s]
u : velocity vector [m/s]
u_{max} : the maximum of x-directional velocity [m/s]
$\overline{u}$: the average velocity of the fluid [m/s]
∇u : the gradient of velocity
W : the width of mixing element [m]
z : the position vector

Greek Letters

γ : shear rate [s^{-1}]
δ : Lyapunov exponent
δ_b : blade thickness [m]
θ : twist angle [deg]
λ : accumulated stretching
Λ : stretching rate at a given cross-section
μ : fluid viscosity [kg/m·s]
ρ : fluid density [kg/m^3]
τ : stress tensor
η : mixing performance factor

REFERENCES

1. R. K. Rahmani, T. G. Keith and A. Ayasoufi, *J. Fluids Eng.*, **128**, 467 (2006).
2. M. Regner, K. Östergren and C. Trägårdh, *Ind. Eng. Chem. Res.*, **47**, 3030 (2008).
3. M. Regner, K. Östergren and C. Trägårdh, *Chem. Eng. Sci.*, **61**, 6133 (2006).
4. R. K. Thakur, C. H. Vial, K. D. P. Nigam, E. B. Nauman and G. D. Jelveh, *Chem. Eng. Res. Des.*, **81**, 787 (2003).
5. A. Ghanem, T. Lemenand, D. D. Valle and H. Peerhossaini, *Chem. Eng. Res. Design*, **92**, 205 (2014).
6. F. Zidouni, E. Krepper, R. Rzehak, S. Rabha, M. Schubert and U. Hampel, *Chem. Eng. Sci.*, **137**, 476 (2015).
7. D. M. Hobbs and F. J. Muzzio, *Chem. Eng. J.*, **67**, 153 (1997).
8. D. M. Hobbs and F. J. Muzzio, *AIChE J.*, **43**, 3121 (1997).
9. D. M. Hobbs and F. J. Muzzio, *Chem. Eng. Sci.*, **53**, 3199 (1998).
10. D. M. Hobbs and F. J. Muzzio, *Chem. Eng. Sci.*, **70**, 93 (1998).
11. E. Fourcade, R. Wadley, H. C. J. Hoefsloot, A. Green and P. D. Iedema, *Chem. Eng. Sci.*, **56**, 6729 (2001).
12. R. K. Rahmani, T. G. Keith and A. Ayasoufi, *J. Fluids Eng.*, **127**, 467 (2005).
13. P. F. Lisboa, J. Fernandes, P. C. Simões, J. P. B. Mota and E. Saatdjian, *J. Supercriti. Fluids*, **55**, 107 (2010).
14. E. Saatdjian, A. J. S. Rodrigo and J. P. B. Mota, *Chem. Eng. J.*, **187**, 289 (2012).
15. V. Kumar, V. Shirke and K. D. P. Nigam, *Chem. Eng. J.*, **139**, 284 (2008).
16. Z. Jaworski, P. Pianko-Opyrch, D. L. Marchisio and A. W. Nienow, *Chem. Eng. Res. Des.*, **85**, 753 (2007).
17. H. Tajima, A. Yamasaki, F. Kiyono and H. Teng, *AIChE J.*, **50**, 871 (2004).
18. H. Tajima, A. Yamasaki and F. Kiyono, *Energy Fuels*, **19**, 2364 (2005).
19. H. Tajima, A. Yamasaki, F. Kiyono and H. Teng, *AIChE J.*, **52**, 2991 (2006).

20. H. Tajima, Y. Yoshida, S. Abiko and K. Yamagiwa, *Chem. Eng. J.*, **156**, 479 (2010).
21. A. Ujhidy, J. Nemeth and J. Szepvolgyi, *Chem. Eng. Process.*, **42**, 1 (2003).
22. E. Lang, P. Drtina, F. Streiff and M. Fleischli, *Int. J. Heat Mass Transfer*, **38**, 2239 (1995).
23. E. S. Mickaily-Huber, F. Bertrand, P. Tanguy, T. Meyer, A. Renken, F. S. Rys and M. Wehrli, *Chem. Eng. J. and Biochem. Eng. J.*, **63**, 117 (1996).
24. J. M. Zalc, E. S. Szalai, F. J. Muzzio and S. Jaffer, *AIChE J.*, **48**, 427 (2002).
25. K. Hirech, A. Arhaliass and J. Legrand, *Ind. Eng. Chem. Res.*, **42**, 1478 (2003).
26. S. Rabha, M. Schubert, F. Grugel, M. Banowski and U. Hampel, *Chem. Eng. J.*, **262**, 527 (2015).
27. H. B. Meng, F. Wang, Y. F. Yu, M. Y. Song and J. H. Wu, *Ind. Eng. Chem. Res.*, **53**, 4084 (2014).
28. H. B. Meng, M. Y. Song, Y. F. Yu, F. Wang and J. H. Wu, *Can. J. Chem. Eng.*, **93**, 1849 (2015).
29. Y. F. Yu, H. Y. Wang, M. Y. Song, H. B. Meng, Z. Y. Wang and J. H. Wu, *Appl. Therm. Eng.*, **94**, 282 (2016).
30. Y. G. Lei, C. H. Zhao and C. F. Song, *Chem. Eng. Technol.*, **35**, 2133 (2012).
31. H. B. Meng, G. X. Zhu, Y. F. Yu, Z. Y. Wang and J. H. Wu, *Int. J. Heat Mass Transfer*, **99**, 647 (2016).
32. S. J. Curran, R. E. Hayes, A. Afacan, M. C. Williams and P. A. Tanguy, *Ind. Eng. Chem. Res.*, **39**, 195 (2000).
33. A. Bakker and L. E. Gates, *Chem. Eng. Prog.*, **91**, 25 (1995).
34. D. Rauline, P. A. Tanguy, J. LeBlevec and J. Bousquet, *Can. J. Chem. Eng.*, **76**, 527 (1998).
35. N. I. Heywood, L. J. Viney and I. W. Stewart, *Fluid Mixing II*, 147 (1984).
36. ANSYS Inc., ANSYS ICEM CFD Help Manual. ANSYS Inc. Southpointe 2600 ANSYS Drive Canonsburg, PA, U.S.A. (2015).
37. Y. Cengel and A. Ghajar, Heat and Mass Transfer: Fundamentals and Applications, McGraw-Hill Science/Engineering/Math, USA (2014).
38. H. P. Grace, *Chem. Eng. Commun.*, **14**, 225 (1982).
39. M. Heniche, P. A. Tanguy, M. F. Reeder and J. B. Fasano, *AIChE J.*, **51**, 44 (2005).
40. ANSYS Inc., ANSYS Fluent User's Guide. ANSYS Inc. Southpointe 2600 ANSYS Drive Canonsburg, PA, U.S.A. (2015).
41. J. M. Ottino, The kinematics of mixing: stretching, chaos, and transport, Cambridge University Press, Cambridge (1989).
42. D. Rauline, J.-M. LE Blévec, J. Bousquet and P. A. Tanguy, *Chem. Eng. Res. Des.*, **78**, 389 (2000).
43. M. Liu, R. L. Peskin, F. J. Muzzio and C. Leong, *AIChE J.*, **40**, 1273 (1994).
44. M. Liu, F. J. Muzzio and R. L. Peskin, *Chaos Solitons & Fractals*, **4**, 2145 (1994).